

Using At-Sensor Radiance and Reflectance Tasseled Cap Transforms Applied to Change Detection for the ASTER Sensor



Lance D. Yarbrough
Greg Easson
Joel S. Kuzmaul

Department of Geology and Geological Engineering
The University of Mississippi
University, Mississippi USA
lance@yarbrough.com
geasson@olemiss.edu
kuzmaul@olemiss.edu

Abstract—The Tasseled Cap Transform (TCT) was originally created for agricultural land investigations. It is a vegetative index commonly used as an indicator of vegetation health and assessing vegetation and land cover change. The nature of the TCT requires linear combinations specific to each sensor. Additionally, the varying units of the reported digital number (DN) require supplementary eigenvectors. TCTs were derived for the at-sensor radiance and at-sensor reflectance and compared using differing change detection application in Mississippi. The Tasseled Cap Soil Brightness Index (SBI) and the Greenness Vegetative Index (GVI) were conducted and evaluated. It was found that the at-sensor radiance based TCT was most useful in a change detection analysis. The desired spectral characteristics were well contrasted while the at-sensor reflectance based TCT tended to be less effective.

Tasseled Cap, ASTER, at-sensor reflectance, at-sensor radiance, vegetative index, eigenspace, solar irradiance

I. INTRODUCTION

The Tasseled Cap Transform (TCT) was originally created [8] for agricultural land investigations. The TCT is a vegetative index commonly used as an indicator of vegetation health and assessing vegetation and land cover change [2]-[6],[12]. There are goals in applying the transform: (1) the multispectral data are rotated in eigenspace and aligned with physical characteristics of the scene and (2) the variance of the data is compressed into a smaller spectral space. This compressed space has been described [8] and is defined by the coordinate axes: Brightness, Greenness, and Wetness. These outcomes enhance the interpretability of the scene and offer smaller input sets for models and analysis methods. Typically, over 95% of variance in a multivariate dataset can be explained by the first three coordinate axes of the TCT's defined feature space [6],[7],[12].

In recent literature, the uses and derivations of the TCT have been applied to a new generation of multispectral sensors.

This paper reports the TCT coefficients for the at-sensor radiance (L_p) and at-sensor reflectance (ρ_p) data models for the Advanced Spaceborne Thermal Emission and Reflection Radiometer (ASTER) sensor currently aboard NASA's TERRA platform. ASTER is an experimental instrument that has 14 spectrally calibrated bands that are similar in bandwidth to the ETM+ sensor aboard the Landsat 7 platform. Descriptions of ASTER's specifications and bandwidth characteristics are available [1] and the TCT coefficients for the digital number (DN) based ASTER L-1B product have been reported [12]. Our paper continues to make use of the same ASTER data granules and methods developed in [12] so that an accurate comparison can be drawn from the two approaches used.

After the TCTs were derived for the at-sensor radiance and at-sensor reflectance data models, a comparison was made using the TCT-based Soil Brightness Index (SBI) and the Green Vegetation Index (GVI). A temporal series of ASTER images were analyzed for the 2001 growing season in the west-central region of Mississippi.

II. METHODS

Because ASTER data contains three pixel resolutions, there is a need to fuse the three bands of 15-m visible infrared (VNIR) data with the six bands of 30-m shortwave infrared (SWIR) data. This will result in a single 30-m image with nine spectrally calibrated bands [1].

A. At-sensor Radiance

Our derivations require that each of the ASTER L-1Bv003 granules be converted to at to at-sensor radiance using the linear relationship [9]:

$$L_\lambda = C_{\lambda,m}(DN_{\lambda,m} - 1) \quad (1)$$

Research sponsored in part by the Enterprise for Innovative Geospatial Solutions (EIGS) (www.eigs.olemiss.edu) and The University of Mississippi Geoinformatics Center (UMGC) (www.umgc.olemiss.edu).

where $DN_{\lambda,m}$ is the digital number of a particular band, λ for a given gain and product version. $C_{\lambda,m}$ is the band and gain specific conversion coefficient and L_{λ} is the at-sensor radiance. There are import utilities available in many commercial software packages that properly account for the date of the imagery acquisition and read the EOS-HDF file for the correct conversion coefficient. If however, there is need for the coefficients, they are reported at [9].

B. At-sensor Reflectance

To reduce the variability between scenes, the at-sensor reflectance was calculated. This step normalizes for the solar irradiance by converting at-sensor radiance to planetary reflectance. The at-sensor reflectance is estimated by [6] by accounting for the effect of incident solar irradiance, reducing the terms to a unitless ratio or percentage:

$$\rho_p = \pi \cdot d^2 \cdot L_{\lambda} \cdot (E_{\text{sun},\lambda} \cdot \cos(\theta_{\text{sz}}))^{-1} \quad (2)$$

where d is the astronomical distance of the Earth to the sun, which can be estimated using [10]; θ_{sz} is the solar zenith angle, $E_{\text{sun},\lambda}$ is the solar spectral irradiance listed in Table I and ρ_p is the at-sensor reflectance. Throughout the literature when dealing with space-borne platforms the term *at-sensor* can also be referred to as *top-of-atmosphere*, *exo-atmospheric*, and *planetary*, hence the subscript p to distinguish the specific locale of the reflectance or radiance measure.

The spectral solar irradiance ($E_{\text{sun},\lambda}$) was derived for each ASTER band using the World Radiation Center (WRC) data set [11], which is used by the ASTER Calibration Team. The spectral solar irradiance values for ASTER bands 1-9 are reported in Table I.

TABLE I. DERIVED SOLAR SPECTRAL IRRADIANCE FOR ASTER

ASTER Band Number	Solar Spectral Irradiance in $\text{W}\cdot\text{m}^{-2}\cdot\mu\text{m}^{-1}$
ASTER 1	1844.6
ASTER 2	1556.5
ASTER 3N	1083.8
ASTER 4	232.74
ASTER 5	79.854
ASTER 6	74.752
ASTER 7	68.898
ASTER 8	60.002
ASTER 9	57.652

WRC data adapted from [11].

C. Derivation of Coefficients

The at-sensor radiance and at-sensor reflectance TCT coefficients were derived [12] for the L1-B v003 data product of the ASTER sensor. We have selected five geographic locations from the Midwest with agricultural landuse. At each of these locations, two nearly cloud-free scenes were selected.

TABLE II. ASTER GRANULES USED IN COEFFICIENT DERIVATION

ASTER Data Granule ID	Location	Date
SC:AST_L1B.003:2017828936	Beatrice, Nebraska	22 March 2001
SC:AST_L1B.003:2016503822	Beatrice, Nebraska	04 September 2000
SC:AST_L1B.003:2017007671	Enid, Oklahoma	21 November 2000
SC:AST_L1B.003:2018236238	Enid, Oklahoma	03 July 2001
SC:AST_L1B.003:2019088608	Kokomo, Indiana	26 January 2002
SC:AST_L1B.003:2003316394	Kokomo, Indiana	16 June 2001
SC:AST_L1B.003:2006256237	Sauk Centre, Minnesota	26 August 2000
SC:AST_L1B.003:2016792422	Sauk Centre, Minnesota	20 October 2000
SC:AST_L1B.003:2018288846	Western Mississippi	18 July 2001
SC:AST_L1B.003:2018742546	Western Mississippi	07 November 2001

Includes five geographic locations, with a leaf-on and leaf-off scene for each.

One scene represents near-peak crop canopy and leaf-on conditions, the other scene represents mostly fallow fields or leaf-off conditions and both are listed in Table II.

The original TCT coefficients [8] referred to the transform space as the fixed feature space, which has its coordinate axes aligned in the Tasseled Cap directions (e.g. Brightness, Greenness, Wetness). To accomplish this rotation, the linear transform has been defined [8] as:

$$\mathbf{u} = \mathbf{W}_{\text{TC}} \cdot \mathbf{x} + \mathbf{r} \quad (3)$$

where \mathbf{x} is the DN value of the fused VNIR and SWIR data, \mathbf{W}_{TC} is the unitary (or orthogonal) transform matrix, and the vector \mathbf{r} is an offset vector that was used to both maintain positive coordinate values of TCT vector \mathbf{u} and to compare TCTs from one sensor to another [7],[12].

The initial eigenvectors were derived using a covariance-based Principle Components Transform (PCT) [3]-[8],[12]. The angles, ϕ_j required to rotate each of the data models into the define feature space of Tasseled Cap space are reported in Table III.

TABLE III. ROTATIONS USED ON THE INITIAL PCT-DERIVED EIGENVECTORS

Rotational Angles ϕ_j	
Radiance Based	Reflectance Based
+160° Rotation about axis ₂	-140° Rotation about axis ₁
-20° Rotation about axis ₃	+75° Rotation about axis ₂
-8° Rotation about axis ₁	

+ (Counter-clockwise)

TABLE IV. TASSELED CAP TRANSFORM COEFFICIENTS FOR ASTER AT-SENSOR RADIANCE

Axis	ASTER 1	ASTER 2	ASTER 3N	ASTER 4	ASTER 5	ASTER 6	ASTER 7	ASTER 8	ASTER 9
Brightness	0.634	0.625	0.446	0.093	-0.015	0.006	0.000	-0.001	-0.001
Greenness	0.047	-0.576	0.632	0.511	-0.065	0.008	0.003	-0.004	-0.003
Wetness	0.768	-0.498	-0.351	-0.198	-0.007	-0.002	-0.002	-0.001	0.003
Fourth	-0.083	-0.141	0.464	-0.774	-0.392	-0.027	-0.016	-0.062	0.038
Fifth	-0.010	-0.052	0.132	-0.175	0.482	0.534	0.551	-0.267	-0.236
Sixth	-0.009	-0.0527	0.143	-0.176	0.406	-0.309	0.124	0.782	-0.242
Seventh	-0.009	-0.048	0.124	-0.144	0.483	0.362	-0.630	0.070	0.442
Eighth	-0.003	-0.032	0.083	-0.088	0.366	-0.488	-0.351	-0.512	-0.476
Ninth	0.000	-0.019	0.054	-0.045	0.277	-0.500	0.400	-0.215	0.680

Radiance values must be in the units of $W/(m^2 \cdot sr^{-1} \cdot \mu m^{-1})$ before the application of the coefficients.

TABLE V. TASSELED CAP TRANSFORM COEFFICIENTS FOR ASTER AT-SENSOR REFLECTANCE

Axis	ASTER 1	ASTER 2	ASTER 3N	ASTER 4	ASTER 5	ASTER 6	ASTER 7	ASTER 8	ASTER 9
Brightness	-0.274	0.676	0.303	-0.256	-0.020	0.415	-0.255	0.073	-0.262
Greenness	-0.006	-0.648	0.564	0.061	-0.055	0.394	-0.193	0.021	-0.249
Wetness	0.166	-0.087	-0.703	0.187	0.040	0.500	-0.287	0.030	-0.318
Fourth	0.384	0.319	0.282	0.748	0.205	0.086	0.134	-0.205	-0.049
Fifth	0.412	0.049	0.076	-0.146	-0.103	-0.021	-0.688	-0.265	0.496
Sixth	0.456	0.064	0.094	-0.040	0.030	-0.180	-0.109	0.849	-0.111
Seventh	0.429	0.074	0.020	-0.212	-0.631	-0.151	0.181	-0.296	-0.474
Eighth	0.355	0.010	0.012	-0.336	0.066	0.570	0.528	0.029	0.389
Ninth	0.251	-0.047	0.033	-0.393	0.734	-0.186	-0.028	-0.270	-0.363

Using a series of rotations in the Principle Component space, the eighty-one components of \mathbf{W}_{TC} were found [12] for the at-sensor radiance and at-sensor reflectance and reported in Tables IV and V, respectively.

D. TCT Based Indices

The matrix \mathbf{W}_{TC} is then used to perform a linear combination of the ASTER data. Each coefficient represents a weighting factor for each of the at-sensor radiance or at-sensor reflectance values. The resulting values are coordinates within Tasseled Cap space. This provides the end-user a meaningful alignment of a condensed feature space where the coordinate axes are aligned in the directions of the Brightness, Greenness, and Wetness.

E. Change Detection Analysis

Four ASTER granules were selected from the west-central Mississippi representing four time periods during the 2001 growing season. The granules were selected for best image quality, minimum cloud cover and maximum time interval between granules. Because the ASTER granule acquisition footprints are not spatially coincident, smaller subsets of the intersecting areas were created. The derived TCTs were then applied to each of the subsets. The result was four temporal images, each transformed to both an at-sensor radiance and an at-sensor reflectance based Tasseled Cap space.

III. RESULTS AND DISCUSSION

Fig. 1 shows the time-series of the at-sensor radiance Tasseled Cap vales. The red hues in the images represent the Brightness coordinate and may be referred to as the Soil Brightness Index (SBI). In the define feature space, the soil line is by definition the Brightness axis of Tasseled Cap space [8]. The green hues of Fig. 1 represent the Greenness coordinate or

Greenness Vegetative Index (GVI) and the blue is assigned to the Wetness coordinate. Early in the growing season, the fields are dominated by large SBI values with exception to the possible rice fields in the in lower right corner of the images.

As the season progresses, the pixels darken and then begin to show larger Greenness values when the crop leaf canopy matures. After summer growth has declined, the field pixels darken representing the wet season in Mississippi.

Fig. 2 graphically illustrates the progression of pixels representing agricultural land use. Each point is the averaged values of twenty randomly selected pixels. The Brightness-Greenness plane of Tasseled Cap space is shown for both the at-sensor radiance (TOP) and at-sensor reflectance (BOTTOM) Tasseled Cap spaces. Note that the at-sensor radiance TCT tends to show the characteristic shape associated with the TCT. The at-sensor reflectance TCT shows a skewed shape in Fig. 2 that is caused by a larger SBI value in the 18 July dated pixels than the early pixels of 29 April.

Compared to previous studies, the at-sensor radiance TCT fits best with other sensors' derivations [3],[6],[12] and [13]. However, the at-sensor reflectance TCT tended to be less useful for detecting change because of the apparent bias evident in the Wetness component of the at-sensor reflectance based TCT. This bias may be attributed to the sensor's lack of recording data from the blue region of the spectrum (450-520 nm) and the additional SWIR bands.

IV. SUMMARY AND CONCLUSIONS

The nature of the Tasseled Cap Transform require linear combinations specific to each sensor. Additionally, the varying units of the reported digital number (DN) require supplementary eigenvectors. This special eigenspace is described by the coordinate axes in the defined Tasseled Cap

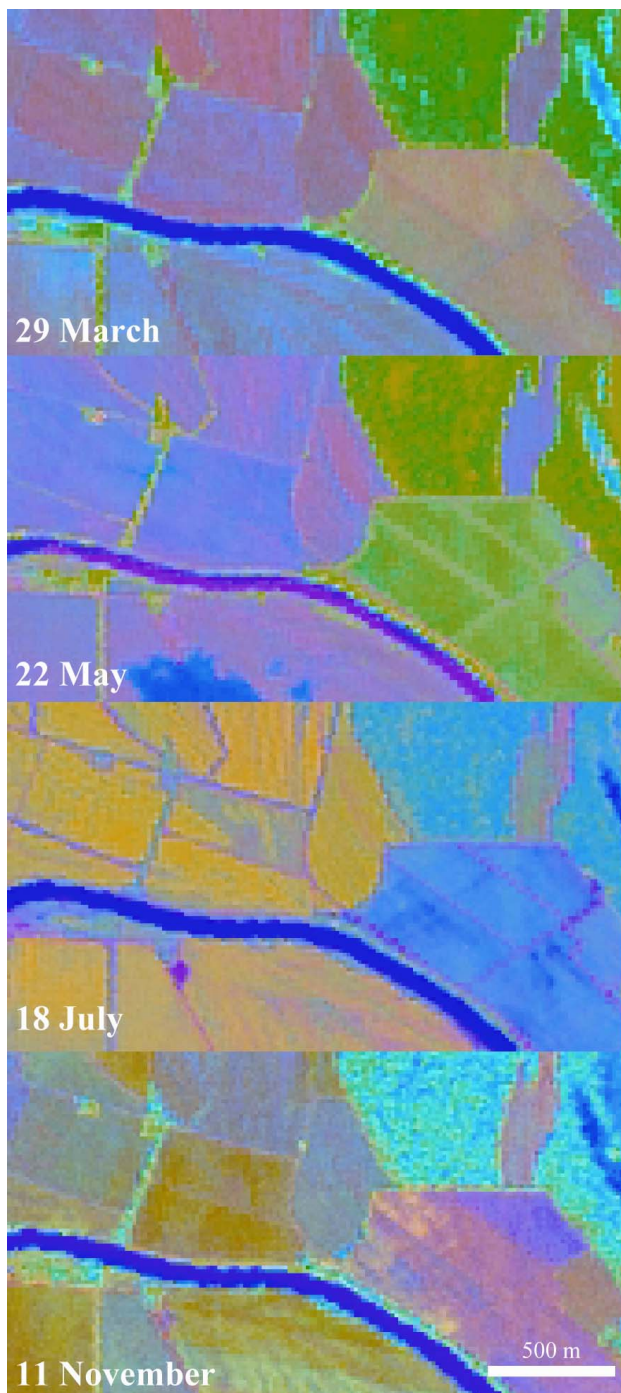


Figure 1. Temporal series of at-sensor radiance Tasseled Cap Transforms.

directions (e.i. Brightness, Greenness, Wetness, etc.). Each TCT matrix is sensor and data-model specific. For every sensor and data type (e.g., radiance, reflectance, DN), a new transform matrix must be derived.

The at-sensor radiance TCT was valuable in analyzing change within an area of forested and agricultural land use. The SBI and GVI using ASTER can be used to track change and establishing of a meaningful change vector.

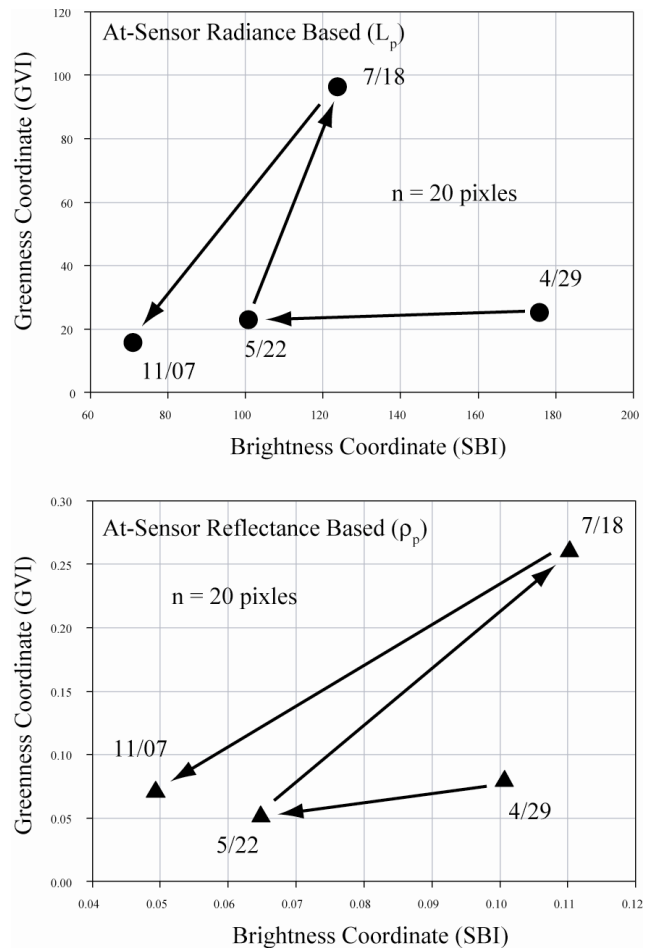


Figure 2. Comparison of at-sensor radiance and reflectance Tasseled Cap Transformed coordinates.

The at-sensor reflectance TCT for ASTER tended to bias the Wetness coordinate and may be attributed to the high negative coefficients in Table V that are not present in Table IV. The effects of the additional SWIR bands are a topic for future research.

V. ACKNOWLEDGMENTS

We would like to thank Ric Cicone and Eric Crist for their thoughtful input on the topic of Tasseled Cap Transforms.

REFERENCES

- [1] M. Abrams, S. Hook, and B. Ramachandran, *ASTER User Handbook, Version 2*, Jet Propulsion Laboratory and EROS Data Center, Pasadena, CA and Sioux Falls, SD, 1999.
- [2] R.C. Cicone, *Personal Communications*.
- [3] E.P. Crist, and R.C. Cicone, "A Physically-Based Transformation of Thematic Mapper Data -- The TM Tasseled Cap," *IEEE Transactions on Geoscience and Remote Sensing*, vol.22, (3), pp. 256-263, 1984.
- [4] E.P. Crist, *Personal Communications*.
- [5] J.H. Horne, "A Tasseled Cap Transform for IKONOS Images," *ASPRS Annual Conference Proceedings*, Anchorage, Alaska, 2003.

- [6] C. Huang, B. Wylie, L. Yang, C. Homer, and G. Zylstra, "Derivation of a tasseled cap transformation based on Landsat 7 at-satellite reflectance," *International Journal of Remote Sensing*, vol. 23, pp. 1741-1748, 2002.
- [7] R.J. Kauth, and E.P. Crist, "The Tasseled Cap DeMystified," *Photogrammetric Engineering and Remote Sensing*, vol. 52, pp. 81-86, 1986.
- [8] R.J. Kauth, and G.S. Thomas, "The Tasseled Cap – A Graphic Description of the Spectral-Temporal Development of Agricultural Crops as Seen by LANDSAT," *Proceedings of the Symposium on Machine Processing of Remotely Sensed Data*, Purdue University, West Layette, Indiana, pp. 4B41-4B51, 1976.
- [9] S. Tsuchida, H. Sakuma, and A. Iwasaki, "Equations for ASTER radiometric calibration, ver.0.20," 2005, from <http://staff.aist.go.jp/s.tsuchida/aster/cal/info/equation/index.html>
- [10] F. Van der Meer, "Spectral mixture modeling and spectral stratigraphy in carbonate lithofacies mapping," *ISPRS Journal of Photogrammetry and Remote Sensing*, vol. 51, pp. 150-162, 1996.
- [11] C. Wehrli, "Extraterrestrial Solar Spectrum," Publication no. 615, *Physikalisch-Meteorologisches Observatorium + World Radiation Center (PMO/WRC) Davos Dorf, Switzerland*, July 1985.
- [12] L.D. Yarbrough, G. Easson, and J.S. Kuzmaul, "DN Based Tasseled Cap Transform Coefficients for the ASTER Sensor Level 1-B Data," unpublished.
- [13] X. Zhang, C.B. Schaaf, M.A. Friedl, A.H. Strahler, F. Gao, and J.C.F.H. Hodges, "MODIS Tasseled Cap Transformation and Its Utility," *Proceedings of the International Geoscience and Remote Sensing Symposium (IGARSS'02)*, Toronto, Canada, pp. 24-28, 2002.